Supporting Information

Designing Core-Shell Metal-Organic Framework Hybrids: Toward High-Efficiency Electrochemical Potassium Storage

Dongbo Yu,[a] Qingjing Song,[a] Jiewu Cui,*[,a] Hongmei Zheng,[a] Yong Zhang,[a] Jiaqin Liu,[a] Jun Lv,[a] Tongwen Xu*[,b] and Yucheng Wu*[,a]

[a] *School of Materials Science and Engineering, Hefei University of Technology, Hefei, 230009, P. R. China*

[b] *CAS Key Laboratory of Soft Matter Chemistry, Collaborative Innovation Center of Chemistry for Energy Materials, School of Chemistry and Material Science, University of Science and Technology of China, Hefei, 230026, P.R. China*

Experimental sections

1. Preparations of core MOFs

1.1 Preparation of 3D Ni-MOF-74 nanoparticles

1 g of $Ni(CH_3COO)_2 \cdot 4H_2O$ and 0.4 g of 2,5-dihydroxybenzenedicarboxylate (DHBDC) were dissolved in 10 ml and 90 ml of deionized water, respectively. Afterwards, the two solution were mixed and placed in 100°C oil bath with magnetic stirring for 40 min. The resulting precipitates were collected by centrifugation, washed with ethanol and water several times, and dried in a 70°C oven. The obtained product were 3D Ni-MOF-74 nanoparticles.

1.2 Preparation of 3D UiO-66 nanoparticles

58.26 mg of $ZrCl_4$ and 41.53 mg of terephthalic acid (H_2BDC) were dissolved in 10 ml of N,N-dimethylformamide (DMF) and then 2.5 ml of acetic acid was added. Subsequently, the resulting mixture was transferred into a Teflon-lined stainless steel autoclave with a capacity of 50 ml, which was then placed in an 180°C oven for 12 h. After cooling down to room temperature, the precipitate was collected by centrifugation and then washed several times with fresh DMF and methanol, and dried in a 70 °C oven, yielding 3D UiO-66 nanoparticles.

1.3 Preparation of 2D ZnCo-TCPP nanosheets

4.05 mg of $Co(NO_3)_2 \cdot 6H_2O$, 0.45 mg of $Zn(NO_3)_2 \cdot 6H_2O$, 1.56 mg of 4,4'-bipyridine and 10 mg of polyvinylpyrrolidone (average mol wt 40,000) were dissolved in 6 ml of the mixture of DMF and ethanol (volume ratio of V_{DMF}:$V_{ethanol}$=3:1) in a 10 ml vial. And the 4.0 mg of 5,10,15,20-tetrakis(4 -carboxylphenyl)-porphyrin (TCPP) dissolved in 2 ml of the mixture of DMF and ethanol (volume ratio of V_{DMF}:$V_{ethanol}$=3:1), which was added dropwisely into the former solution and then sonicated for 25 min. After that, the vial was capped and then heated to 80 ^oC for 24 h. The red ZnCo-TCPP nanosheets were collected by centrifuging at 8000 r. p. m. for 10 min, washed with ethanol several time, and dried at a 70 ^oC oven. Finally, the were obtained.

1.4 Preparation of 1D ZnCo-MOF-74 nanowires

0.18 g of $Zn(CH_3COO)_2 \cdot 2H_2O$ and 0.82 g of $Co(CH_3COO)_2 \cdot 4H_2O$ were dissolved in 10 ml of deionized water, which was then added into 90 ml of 0.4 g DHBDC

aqueous solution. The mixture was heated at 100°C for 40 min with magnetic stirring. The earth yellow precipitate was collected by centrifugation, washed with ethanol and water several times, and dried in a 70 °C oven, yielding 1D ZnCo-MOF-74 nanowires.

1.5 Preparation of 1D Ce-BTC nanowires

0.168 g of 1,3,5-benzenetricarboxylic acid (H_3BTC) and 0.347 g of $Ce(NO_3)_3 \cdot 6H_2O$ were separately dissolved in 20 ml of deionized water, and the two solutions were mixed at 80 °C with magnetic stirring for 20 s. The white 1D Ce-BTC nanowires were collected by centrifugation, washed with ethanol and water several times, and dried in a 70°C oven.

2. Preparations of Ni/Co-containing MOF@ZIF core-shell hybrids

2.1 Preparation of Ni/Co-containing MOF@ZIF@ZIF-8 core-shell hybrids

The prepared core MOFs (102.5 mg of 3D Ni-MOF-74 nanoparticles, 130 mg of 3D UiO-66 nanoparticles, 4.25 mg of 2D ZnCo-TCPP nanosheets, 100 mg of 1D ZnCo-MOF-74 nanowires, 82.5 mg of 1D Ce-BTC nanowires) were first immersed in Hmim methanol solution (respectively 1.5 g of Hmim in 20 ml of methanol, 1.5 g of Hmim in 20 ml of methanol, 0.4 g of Hmim in 25 ml of methanol, 1.84 g of Hmim in 15 ml of methanol, 2 g of Hmim in 20 ml of methanol) with magnetic stirring at room temperature for 10 minutes. Afterwards, $Zn(NO_3)_2 \cdot 6H_2O$ methanol solution (respectively 0.2 g, 0.2 g, 0.1 g, 0.83 g, 0.6 g of $Zn(NO_3)_2 \cdot 6H_2O$ in 5 ml of methanol) was added drop by drop with continuously stirring for another 15 minutes. The resulting products were collected by centrifugation, washed with ethanol and water several times, and dried in a 70°C oven. The MOF core-shell hybrids including 3D Ni-MOF-74@ZIF-8 nanoparticles, 3D UiO-66@ZIF-8 nanoparticles, 2D ZnCo-TCPP@ZIF-8 nanosheets, 1D ZnCo-MOF-74@ZIF-8 nanowires and 1D Ce-BTC@ZIF-8 nanowires were synthesized.

2.2 Preparation of Ni/Co-containing MOF@ZIF@ZIF-67 core-shell hybrids

The prepared core MOFs (102.5 mg of 3D Ni-MOF-74 nanoparticles, 65 mg of 3D UiO-66 nanoparticles, 4.25 mg of 2D ZnCo-TCPP nanosheets, 40 mg of 1D ZnCo-MOF-74 nanowires, 82.5 mg of 1D Ce-BTC nanowires) were first immersed in Hmim methanol solution (respectively 3 g of Hmim in 25 ml of methanol, 4 g of Hmim in 25 ml of methanol, 0.8 g of Hmim in 25 ml of methanol, 0.657 g of Hmim

in 10 ml of methanol, 8 g of Hmim in 25 ml of methanol) with magnetic stirring at room temperature for 10 minutes. Afterwards, $Co(NO_3)_2 \cdot 6H_2O$ methanol solution (respectively 0.1 g, 0.1 g, 0.05 g, 0.025 g, 0.3 g of $Zn(NO_3)_2 \cdot 6H_2O$ in 5 ml of methanol) was added drop by drop with continuously stirring for another 15 minutes. The resulting products were collected by centrifugation, washed with ethanol and water several times, and dried in a 70°C oven. The MOF core-shell hybrids including 3D Ni-MOF-74@ZIF-67 nanoparticles, 3D UiO-66@ZIF-67 nanoparticles, 2D ZnCo-TCPP@ZIF-67 nanosheets, 1D ZnCo-MOF-74@ZIF-67 nanowires and 1D Ce-BTC@ZIF-67 nanowires were synthesized.

3. Preparations of solid ZIF-8 particles

0.878 g of $Zn(CH_3COO)_2 \cdot 2H_2O$ and 3.284 g of 2-methylimidazole (Hmim) were respectively dissolved in 10 ml and 50 ml of H_2O, the former solution was dropped into the latter solution at room temperature with magnetic stirring for 24h. Solid ZIF-8 particles were collected by centrifugation, washed with ethanol and water several times, and dried in a 70°C oven.

4. Preparations of nanoporous carbon derived from MOF precursors

The MOF precursors, including solid ZIF-8 particles, 3D Ni-MOF-74 nanoparticles, 2D ZnCo-TCPP nanosheets, 1D ZnCo-MOF-74 nanowires, 3D Ni-MOF-74@ZIF-8 nanoparticles, 2D ZnCo-TCPP@ZIF-8 nanosheets and 1D ZnCo-MOF-74@ZIF-8 nanowires, were heated to 900 ^oC in an Ar atmosphere for 2 h at a heating rate of 2 ^oC/min. After cooling to room temperature naturally, all the black powders were washed with 5 M HNO_3 aqueous solution at 80 ^oC for 24 h to remove the Zn, Ni or Co species. The resulting materials were collected by centrifugation, washed with ethanol and water several times, and finally dried in a 80 ^oC oven.

5. Material Characterizations

The X-ray diffraction (XRD) characterization was carried out on a Rigaku D/MAX2500VL/PC X-ray diffractometer with Cu Kα radiation. The microstructures of the samples were analyzed by field-emission scanning electron microscopy (SEM, SU8020) and transmission electron microscopy (TEM, JEM-2100). The elemental analysis was conducted on a elemental analyzer (Elementar Vario EL Club). X-ray photoelectron spectroscopy (XPS) was performed by a Thermo Fisher X-ray

photoelectron spectrometer (ESCALAB250), and the results were fitted using XPSpeak software according to the principle of minimum residual standard deviation. The Raman spectrum was recorded from an Ar laser (Renishaw inVia) with a 532 nm laser excitation source at room temperature. Nitrogen adsorption-desorption analysis was conducted by a Micromeritics ASAP 2020 instrument at 77 K, and the surface area values were calculated by the Brunauer-Emmett-Teller (BET) method in the relative pressure (P/P_o) range of 0.002 ~ 1.0.

6. Electrochemical Measurements

The electrochemical K+ storage performance of MOF-derived nanoporous carbon was tested by assembling 2032 type coin cells. For the preparation of working electrodes, the obtained MOF-derived nanoporous carbon were mixed with Super P® carbon black and polyvinylidene fluoride at a weight ratio of 8:1:1 in N-methyl pyrrolidinone (NMP) to make a slurry mixture. Subsequently, the slurry was pasted on a copper foil and dried in a 80 °C vacuum oven for 12 h. The mass loading of the working electrodes ranged from 0.8 to 1.0 mg/cm^2. Metal K foil was used as the counter electrode, and borosilicate glass microfiber (GF/D, Whatman) was used as the separator. The electrolyte was 0.8 M KPF6 in a mixed solution of ethylene carbonate (EC) and diethyl carbonate (DEC) (volume ratio of V_{EC}:V_{DEC} =1:1). The coin cells were assembled in an Ar-filled glovebox (MIKROUNA) and allowed to rest 12 h. The galvanostatic discharge/charge tests were conducted on a Land CT2001A battery tester (China) in a 25 ºC thermostat (FYL-YS-280L, Beijing Fu Italian Electric Co., Ltd., China). The cyclic voltammetry and electrochemical impedance spectroscopy (EIS) curves were recorded on a CHI760E electrochemical workstation (Chenhua Instrument Company, China).

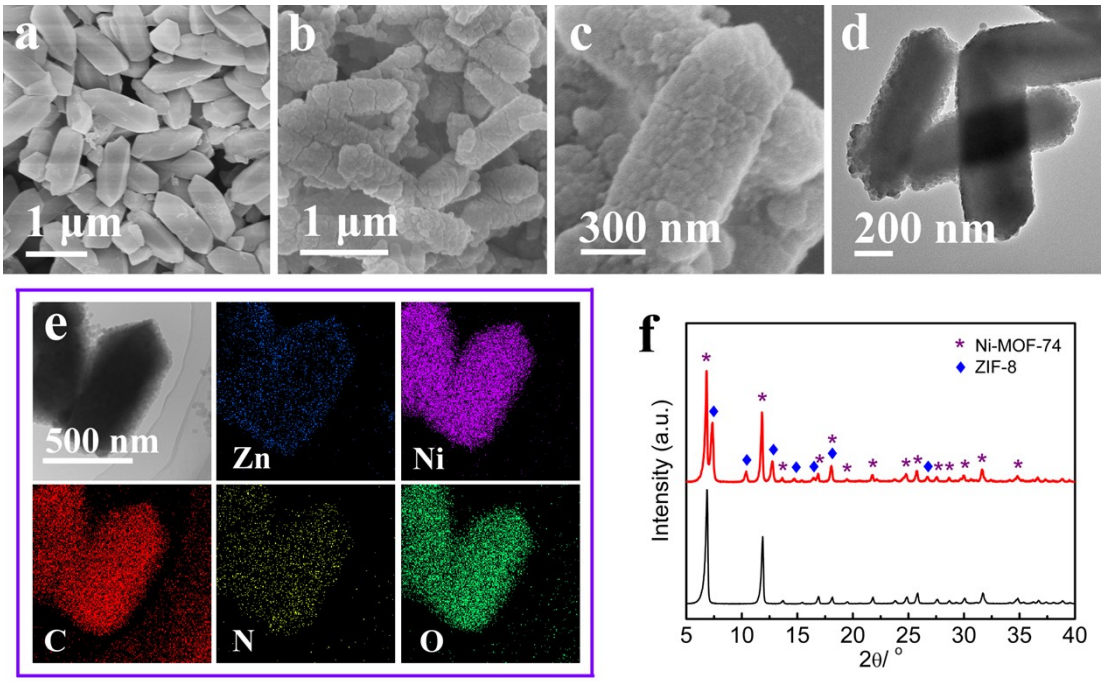

Figure S1 SEM images of Ni-MOF-74 (a) and Ni-MOF-74@ZIF-8 core-shell hybrids (b, c); TEM image (d) and EDX mapping images (e) of Ni-MOF-74@ZIF-8 core-shell hybrids; (f) XRD patterns of materials Ni-MOF-74 (black line) and Ni-MOF-74@ZIF-8 core-shell hybrids (red line).

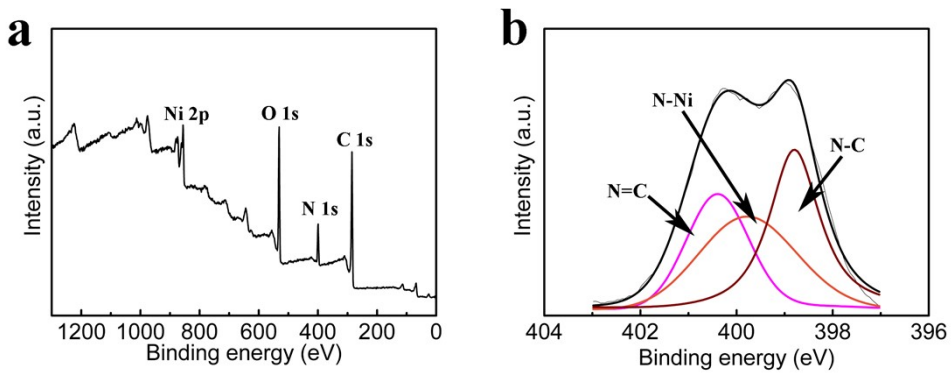

Figure S2 The full (a) and high-resolution N 1s (b) XPS spectra of the resulting materials after Ni-MOF-74 was placed in 0.9 M Hmim methanol solution for 10 mim. The high-resolution N 1s spectrum were fitted with three peaks at approximately 398.8, 399.6 and 400.3 eV. Peaks located at 398.8 and 400.3 eV could be assigned to N-C and N=C of 2-methylimidazole, respectively. The peak at 399.6 eV corresponded to the N-Ni bond, revealing the surface of Ni-MOF-74 was modified by 2-methylimidazole and N-Ni coordination was established, which would lower the energy barrier of heterogeneous nucleation and offer nucleation sites for crystallizing ZIFs.

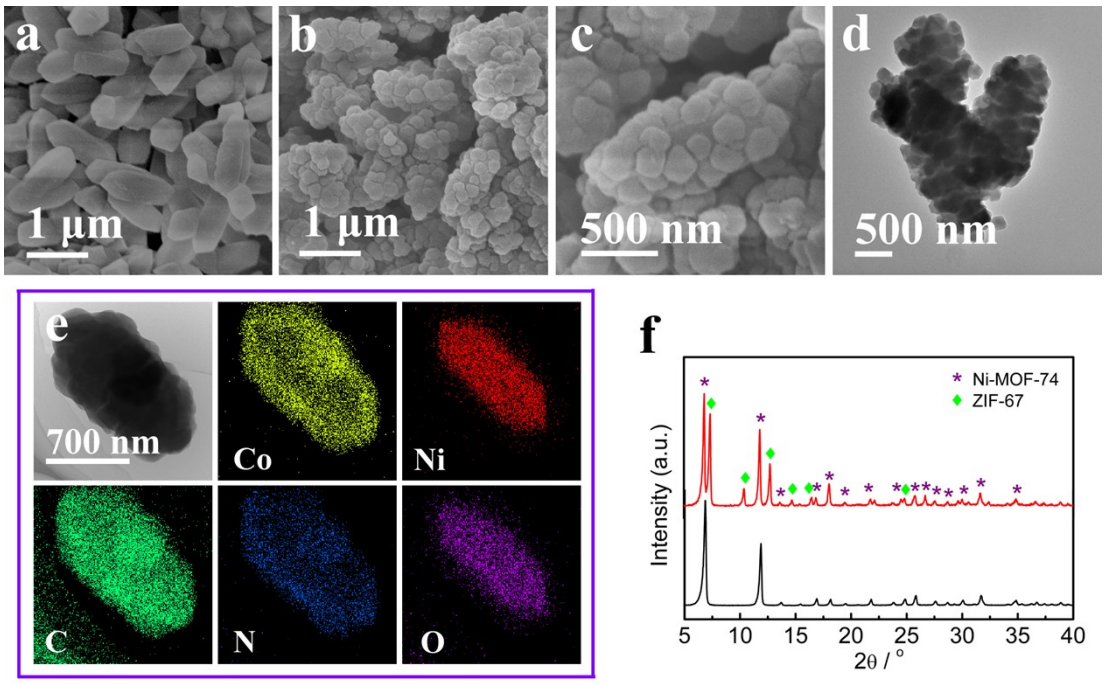

Figure S3 SEM images of Ni-MOF-74 (a) and Ni-MOF-74@ZIF-67 core-shell hybrids (b, c); TEM image (d) and EDX mapping images (e) of Ni-MOF-74@ZIF-67 core-shell hybrids; (f) XRD patterns of materials Ni-MOF-74 (black line) and Ni-MOF-74@ZIF-67 core-shell hybrids (red line).

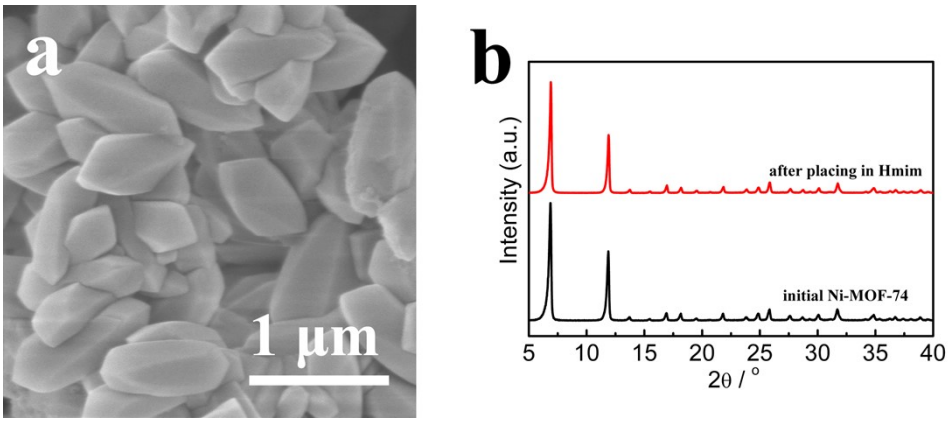

Figure S4 SEM image (a) and XRD pattern (b) of the resulting materials after Ni-MOF-74 nanoparticels were placed in Hmim ethanol solution for 12 h at room temperature. No change was seen in SEM image and XRD results, suggesting ligand exchange could be ignored if Ni-MOF-74 nanoparticels were placed in Hmim ethanol solution for only 15 min.

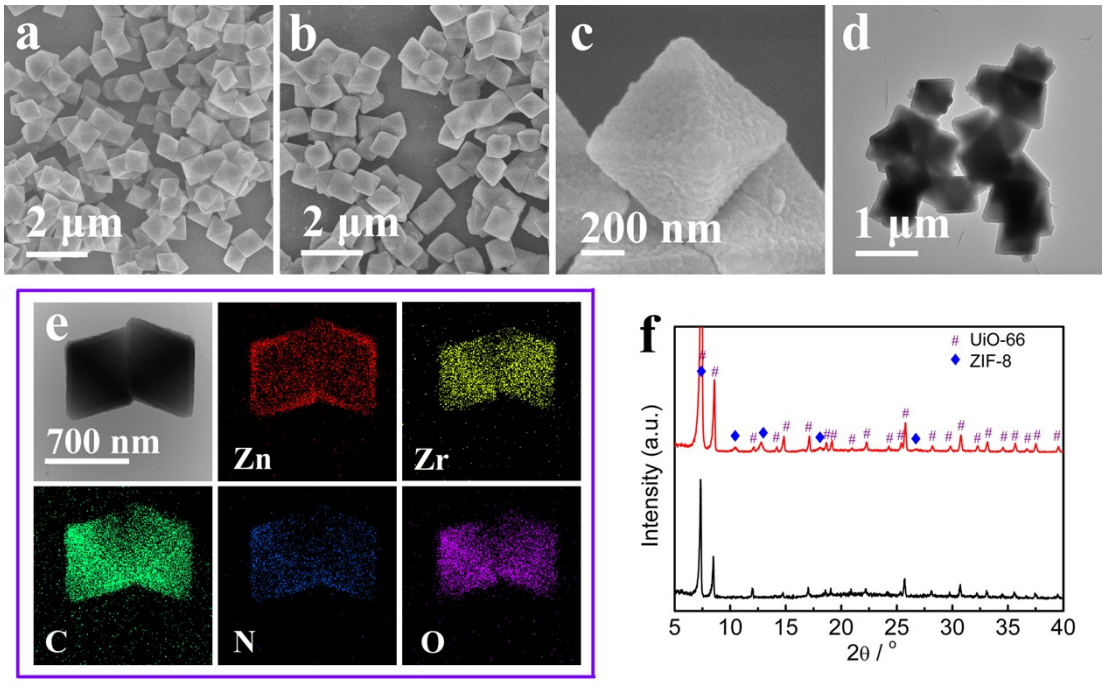

Figure S5 SEM images of UiO-66 (a) and UiO-66@ZIF-8 core-shell hybrids (b, c); TEM image (d) and EDX mapping images (e) of UiO-66@ZIF-8 core-shell hybrids; (f) XRD patterns of materials UiO-66 (black line) and UiO-66@ZIF-8 core-shell hybrids (red line).

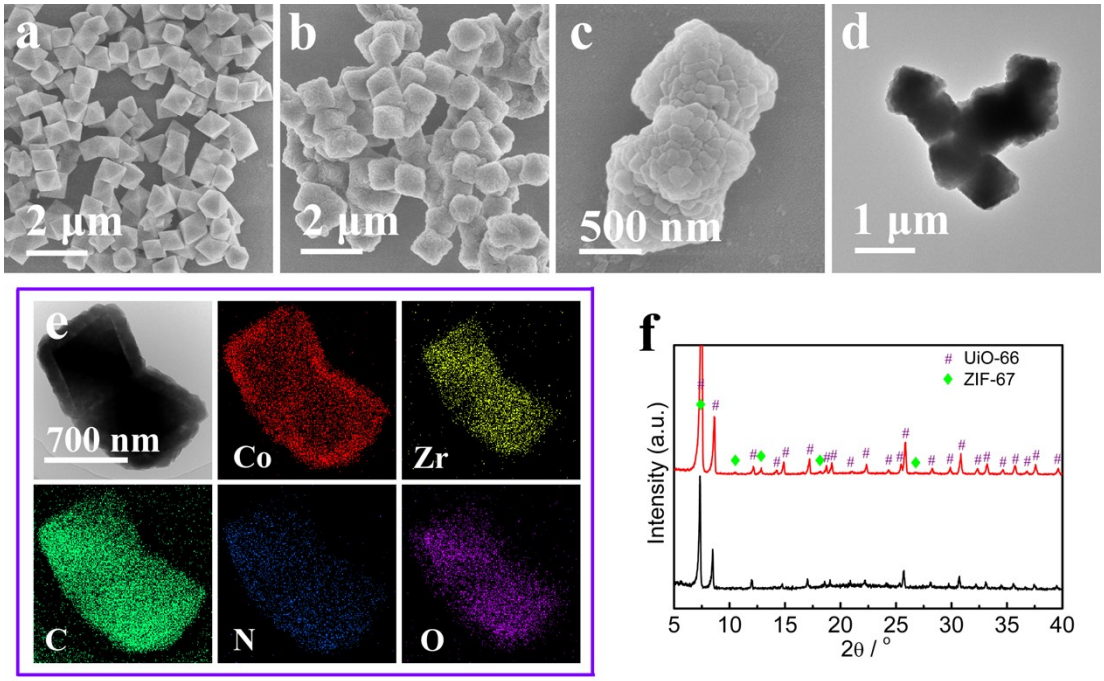

Figure S6 SEM images of UiO-66 (a) and UiO-66@ZIF-67 core-shell hybrids (b, c); TEM image (d) and EDX mapping images (e) of UiO-66@ZIF-67 core-shell hybrids; (f) XRD patterns of materials UiO-66 (black line) and UiO-66@ZIF-67 core-shell hybrids (red line).

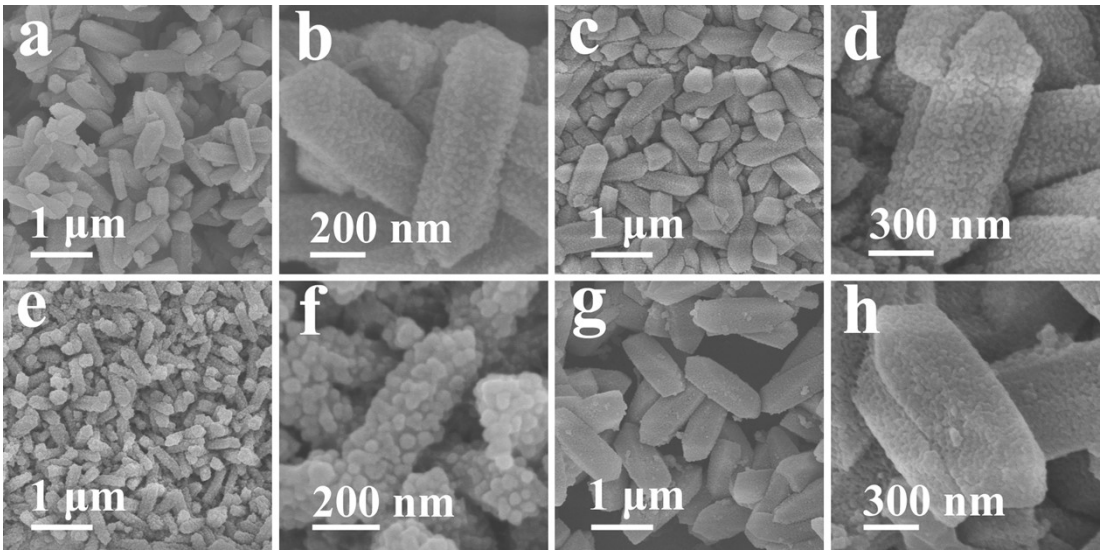

Figure S7 SEM images of the resulting products when Ni-MOF-74 was placed into Hmim methanol solution for 10 min and afterward $Zn(NO_3)_2$ methanol solution was added for 10 s (a, b) and 30 s (c, d); SEM images of the resulting products when Ni-MOF-74 was placed into $Zn(NO_3)_2$ methanol solution for 10 min and afterward Hmim methanol solution was added for 10 s (e,f) and 30 s (g, h). In Figure S7a-d, before $Zn(NO_3)_2$ was added, there would be a concentration gradient of Hmim nearby Ni-MOF-74, and Hmim adsorbed within Ni-MOF-74 reached a maximum value. Once Zn^{2+} ions were added, owing to the diffusing effect of Zn^{2+} and the consumption of deprotonated Hmim (mim^-) for crystallizing ZIF-8, the molar ratio of mim^-/Zn^{2+} would decrease with the time, therefore, the particle size of produced ZIF-8 would become bigger gradually. In contrast, if Ni-MOF-74 was placed into Hmim methanol solution first and $Zn(NO_3)_2$ was added afterward (Figure S7e-h), following the similar principle, the molar ratio of mim^-/Zn^{2+} would increase with the time, therefore, the ZIF-8 particle size would become smaller gradually.

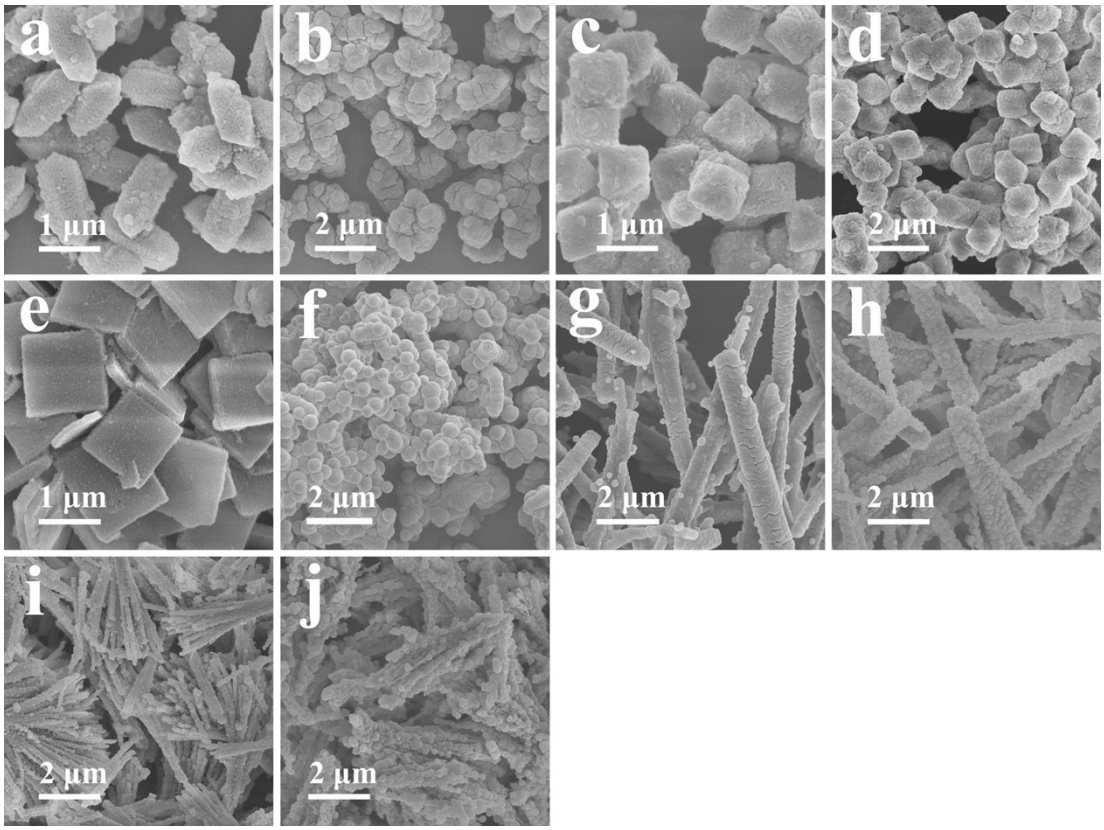

Figure S8 SEM images of the resulting products when the core MOFs were placed into $Zn(NO_3)_2$/$Co(NO_3)_2$ methanol solution for 10 min and afterward Hmim methanol solution was added for another 15 min, still MOF core-shell hybrids could be synthesized: Ni-MOF-74@ZIF-8 (a), Ni-MOF-74@ZIF-67 (b), UiO-66@ZIF-8 (c), UiO-66@ZIF-67 (d), ZnCo-TCPP@ZIF-8 (e), ZnCo-TCPP@ZIF-67 (f), ZnCo-MOF-74@ZIF-8 (g), ZnCo-MOF-74@ZIF-67 (h), Ce-BTC@ZIF-8 (i) and Ce-BTC@ZIF-67 (j). While a few monodispersed ZIF-8/ZIF-67 nanocrystals in the products could be observed. A possible explanation was the initially produced ZIF-8/ZIF-67 were too big to form strong adhesion to the core MOFs, which would fall off with the shell growth process.

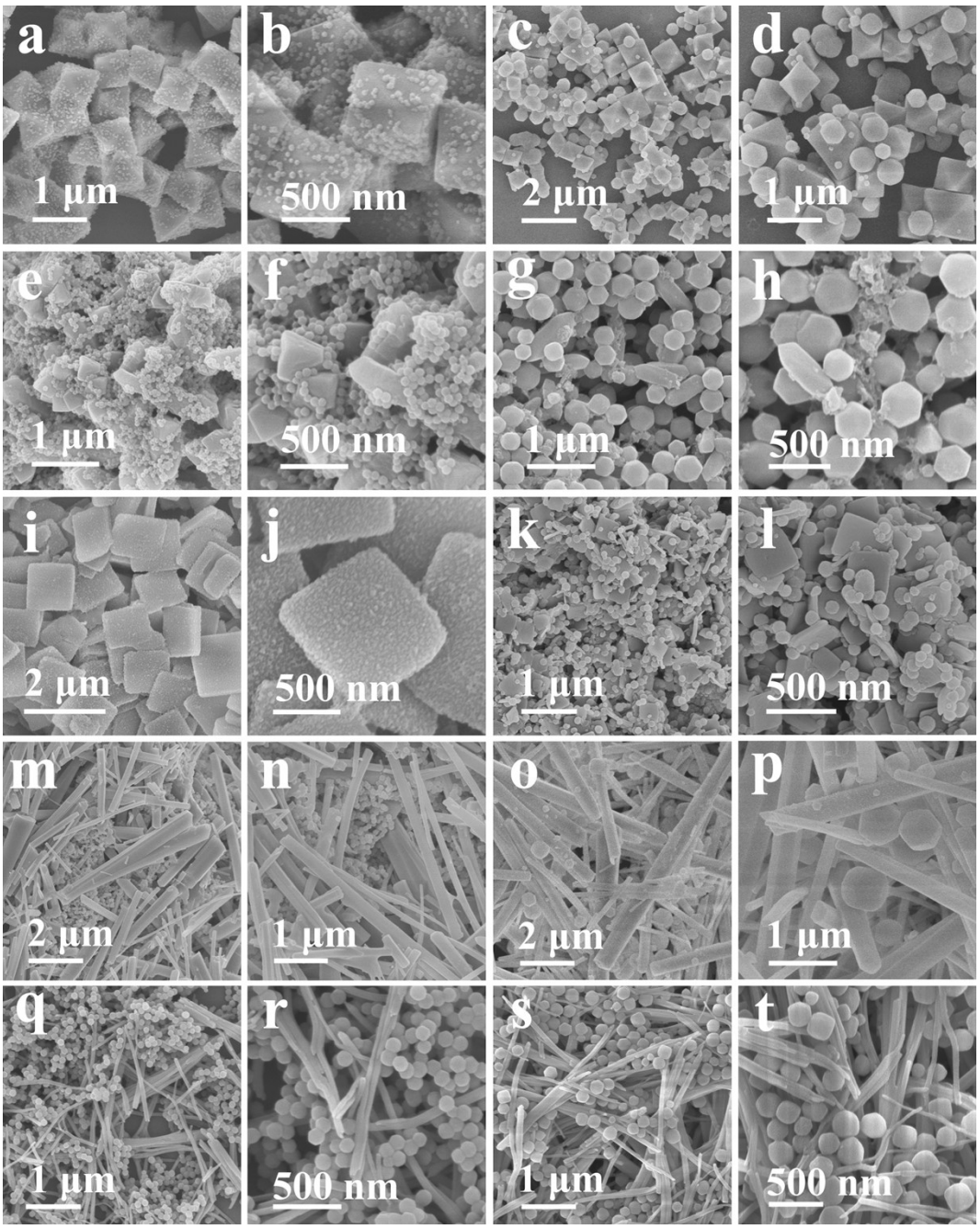

Figure S9 SEM images of the resulting products when core MOFs were placed into mixture solution of $Zn(NO_3)_2$/$Co(NO_3)_2$ and Hmim for 25 min. Basically the resulting products were physical mixtures of core MOFs and shell ZIFs: UiO-66+ZIF-67 (c, d), Ni-MOF-74+ZIF-8 (e, f), Ni-MOF-74+ZIF-67 (g, h), ZnCo-TCPP+ZIF-67 (k, l), ZnCo-MOF-74+ZIF-8 (m, n), ZnCo-MOF-74+ZIF-67 (o, p), Ce-BTC+ZIF-8 (q, r), Ce-BTC+ZIF-67 (s, t), except ZnCo-TCPP@ZIF-8 was obtained (i, j) because the flat plane of nanosheet was more beneficial for crystallization compared to convex plane. Also a spot of ZIF-8 nanocrystals were sporadically distributed on UiO-66 planes (a, b). Due to slower crystallization kinetics, it was not as easy to load ZIF-67 as ZIF-8.

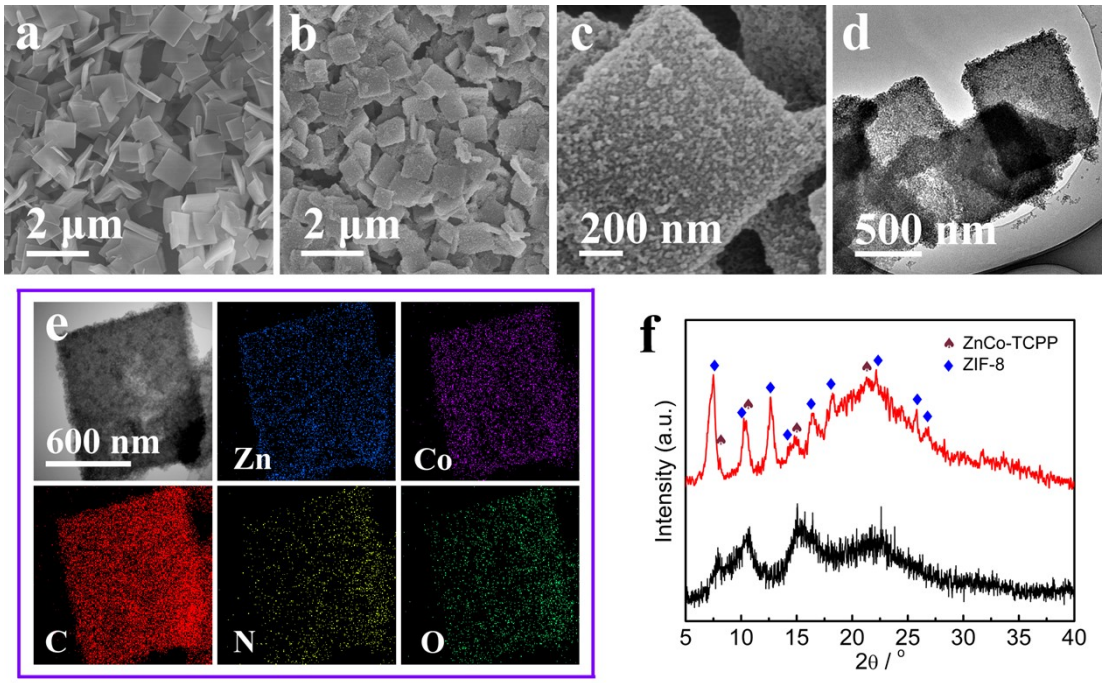

Figure S10 SEM images of ZnCo-TCPP nanosheets (a) and ZnCo-TCPP@ZIF-8 core-shell hybrids (b, c); TEM image (d) and EDX mapping images (e) of ZnCo-TCPP@ZIF-8 core-shell hybrids; (f) XRD patterns of materials ZnCo-TCPP (black line) and ZnCo-TCPP@ZIF-8 core-shell hybrids (red line).

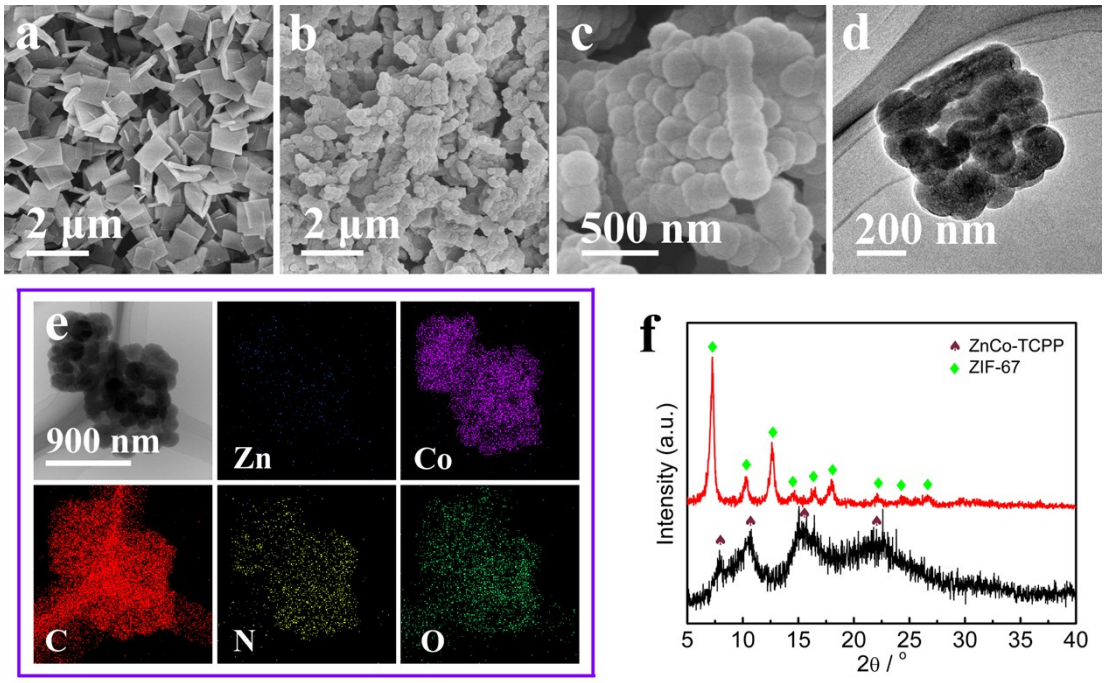

Figure S11 SEM images of ZnCo-TCPP nanosheets (a) and ZnCo-TCPP@ZIF-67 core-shell hybrids (b, c); TEM image (d) and EDX mapping images (e) of ZnCo-TCPP@ZIF-67 core-shell hybrids; (f) XRD patterns of materials ZnCo-TCPP (black line) and ZnCo-TCPP@ZIF-67 core-shell hybrids (red line).

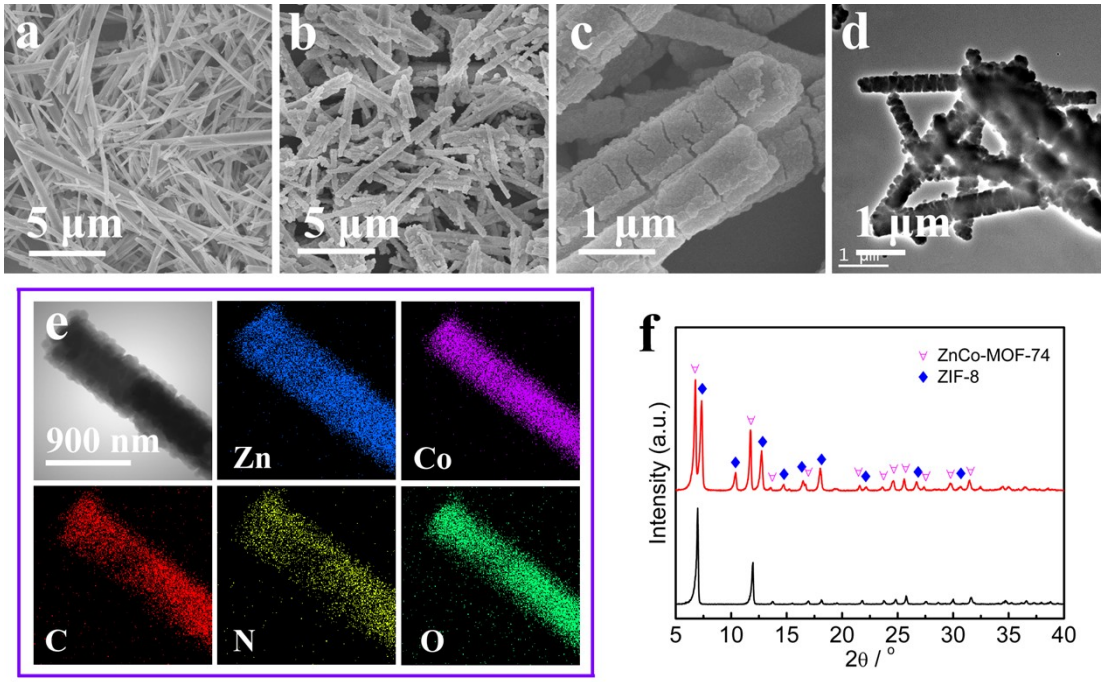

Figure S12 SEM images of ZnCo-MOF-74 nanowires (a) and ZnCo-MOF-74@ZIF-8 core-shell hybrids (b, c); TEM image (d) and EDX mapping images (e) of ZnCo-MOF-74@ZIF-8 core-shell hybrids; (f) XRD patterns of materials ZnCo-MOF-74 (black line) and ZnCo-MOF-74@ZIF-8 core-shell hybrids (red line).

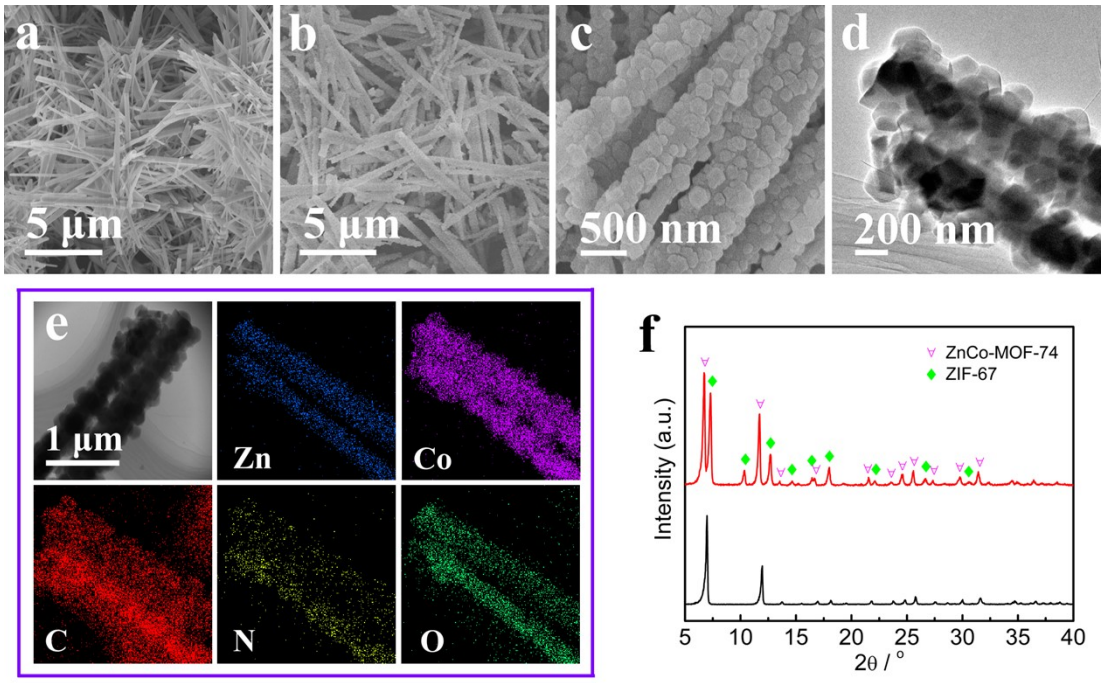

Figure S13 SEM images of ZnCo-MOF-74 nanowires (a) and ZnCo-MOF-74@ZIF-67 core-shell hybrids (b, c); TEM image (d) and EDX mapping images (e) of ZnCo-MOF-74@ZIF-67 core-shell hybrids; (f) XRD patterns of materials ZnCo-MOF-74 (black line) and ZnCo-MOF-74@ZIF-67 core-shell hybrids (red line).

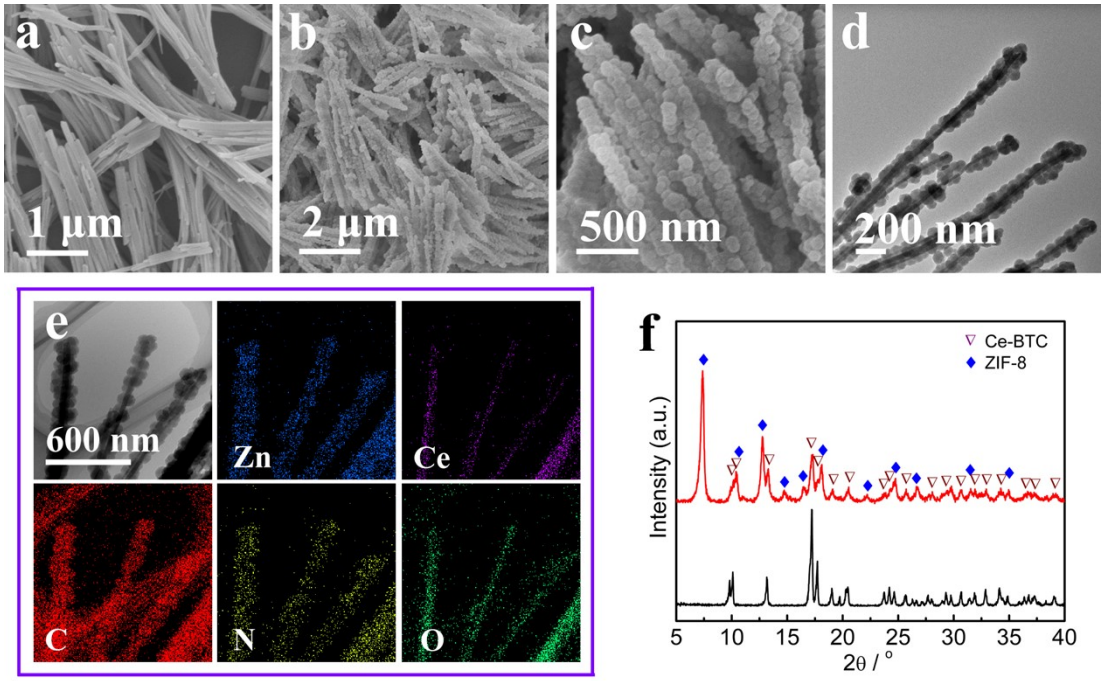

Figure S14 SEM images of Ce-BTC nanowires (a) and Ce-BTC@ZIF-8 core-shell hybrids (b, c); TEM image (d) and EDX mapping images (e) of Ce-BTC@ZIF-8 core-shell hybrids; (f) XRD patterns of materials Ce-BTC (black line) and Ce-BTC@ZIF-8 core-shell hybrids (red line).

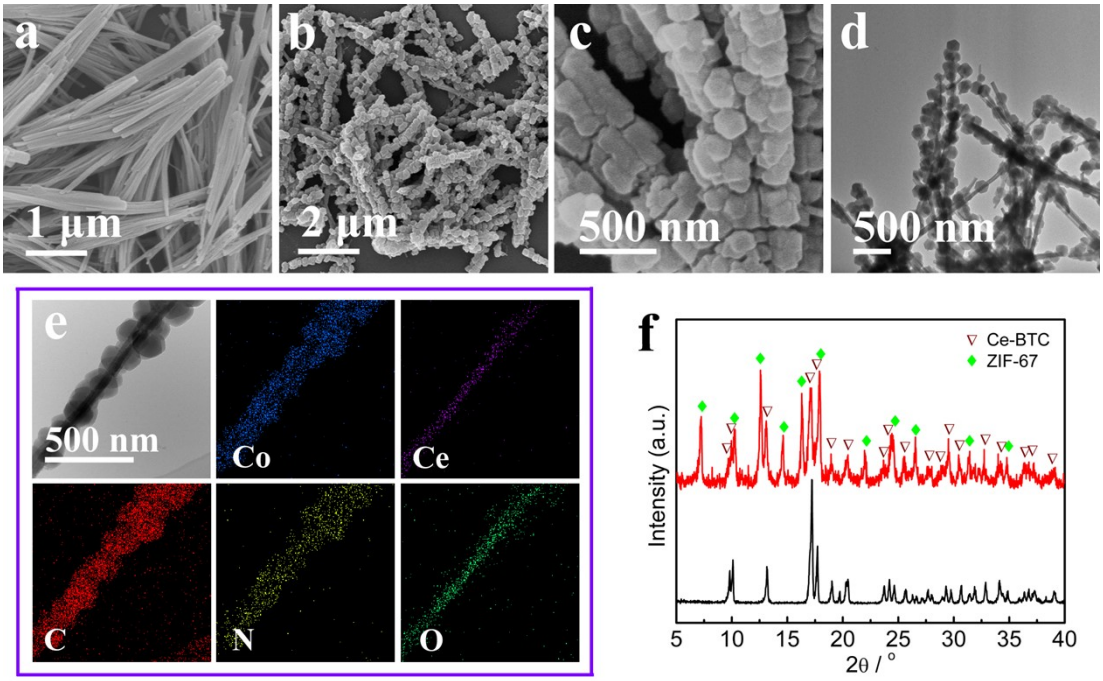

Figure S15 SEM images of Ce-BTC nanowires (a) and Ce-BTC@ZIF-67 core-shell hybrids (b, c); TEM image (d) and EDX mapping images (e) of Ce-BTC@ZIF-67 core-shell hybrids; (f) XRD patterns of materials Ce-BTC (black line) and Ce-BTC@ZIF-67 core-shell hybrids (red line).

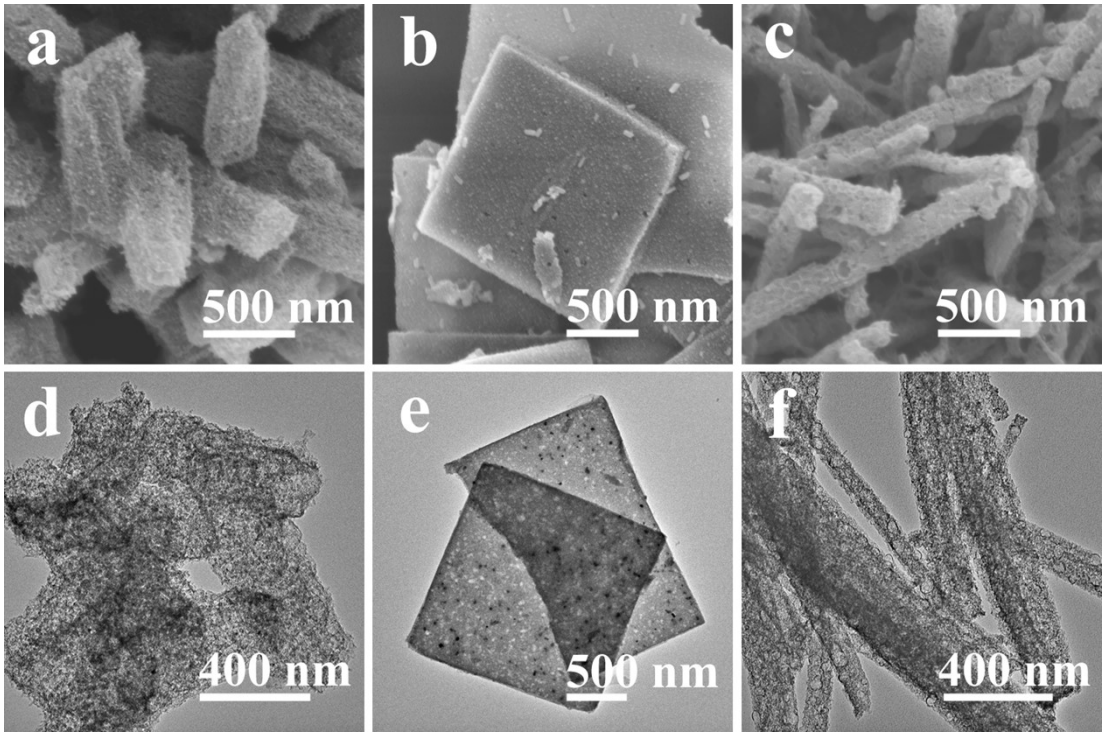

Figure S16 SEM images of 3D Ni-MOF-74-C (a), 2D ZnCo-TCPP-C (b) and 1D ZnCo-MOF-74-C (c); TEM images of 3D Ni-MOF-74-C (d), 2D ZnCo-TCPP-C (e) and 1D ZnCo-MOF-74-C (f).

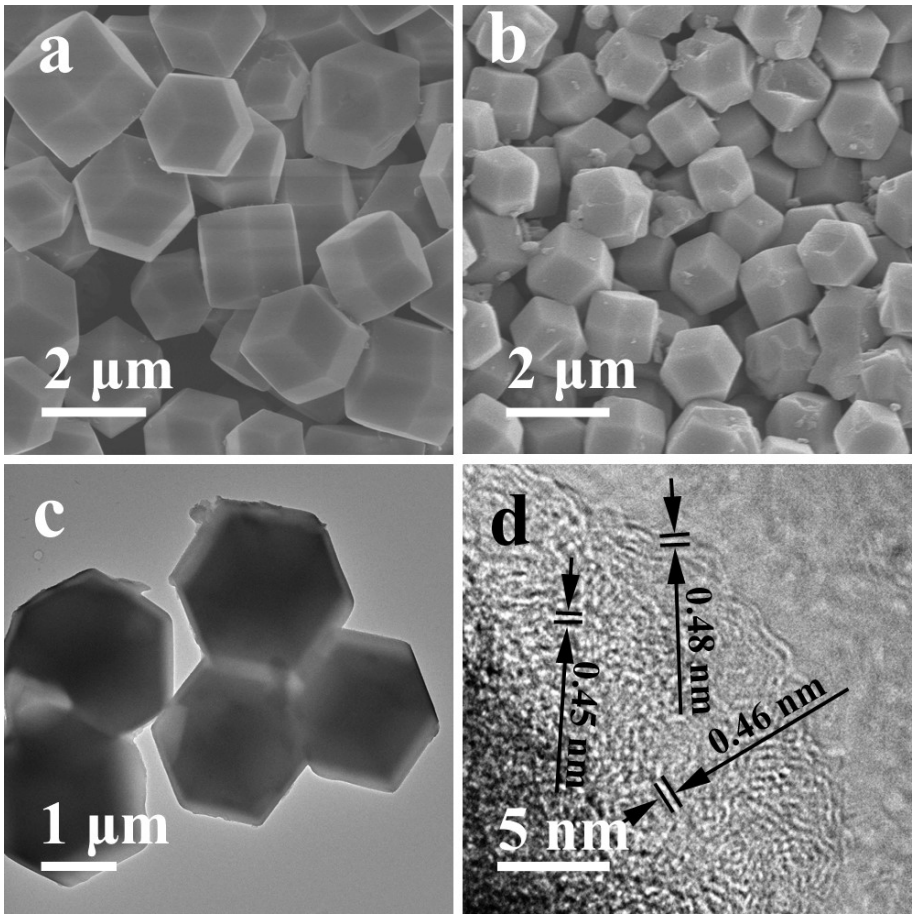

Figure S17 SEM (a, b), TEM (c) and high-resolution TEM (d) images of ZIF-8-C.

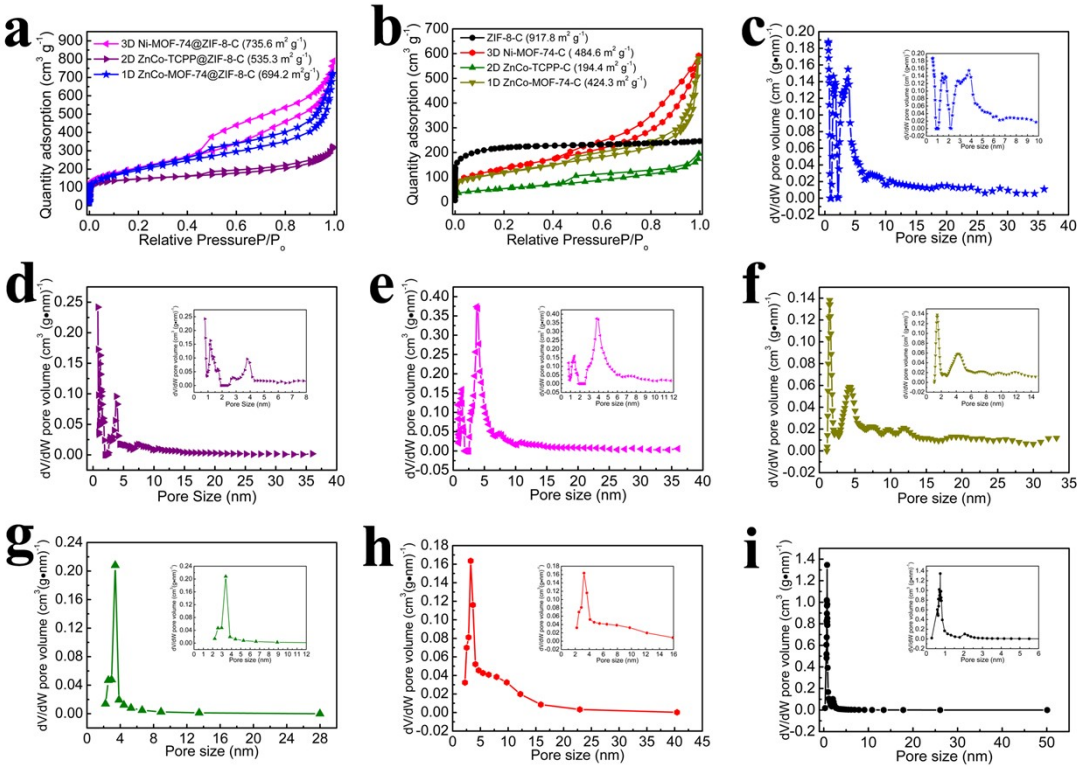

Figure S18 Nitrogen adsorption-desorption isotherms of 1D ZnCo-MOF-74@ZIF-8-C, 2D ZnCo-TCPP@ZIF-8-C, 3D Ni-MOF-74@ZIF-8-C, 1D ZnCo-MOF-74-C, 2D ZnCo-TCPP-C, 3D Ni-MOF-74-C and ZIF-8-C (a, b); the Barrett-Joyner-Halenda pore size distribution plots of 1D ZnCo-MOF-74@ZIF-8-C (c), 2D ZnCo-TCPP@ZIF-8-C (d), 3D Ni-MOF-74@ZIF-8-C (e), 1D ZnCo-MOF-74-C (f), 2D ZnCo-TCPP-C (g), 3D Ni-MOF-74-C (h) and ZIF-8-C (i).

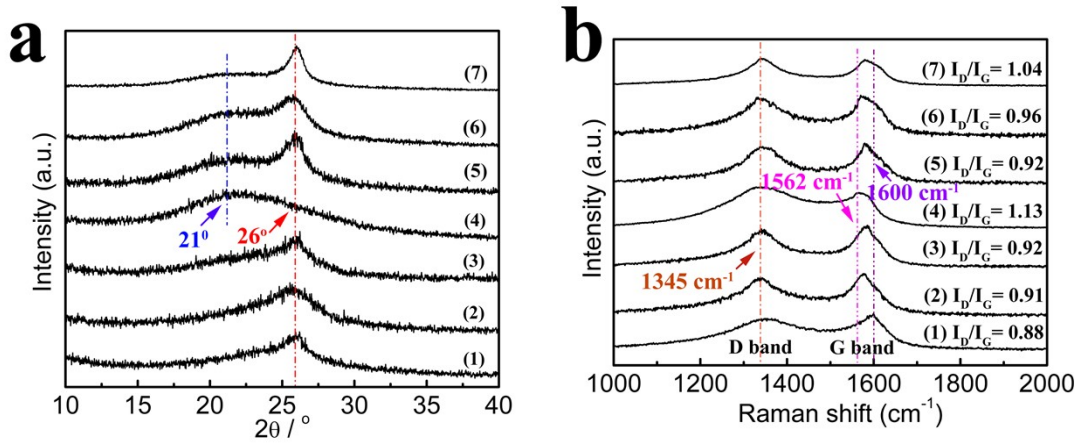

Figure S19 XRD patterns (a) and Raman spectra (b) of MOF-derived nanoporous carbon: 3D Ni-MOF-74-C (1), 2D ZnCo-TCPP-C (2), 1D ZnCo-MOF-74-C (3), ZIF-8-C (4), 3D Ni-MOF-74@ZIF-8-C (5), 2D ZnCo-TCPP@ZIF-8-C (6) and 1D ZnCo-MOF-74@ZIF-8-C (7). In XRD patterns, the more broader C(002) diffraction peaks of 3D Ni-MOF-74-C, 2D ZnCo-TCPP-C, 1D ZnCo-MOF-74-C were located at upper position of ~ 26° compared with that of ZIF-8-C (~ 21°), suggesting that Ni/Co-containing MOFs-derived carbon had higher graphitization degree than ZIF-8-derived counterpart. According to Bragg's equation, The calculated interplanar spacing values of C(002) located at ~ 26° and ~ 21° were respectively 0.342 and 0.423 nm, agreeing with the high-resolution TEM observation. In Raman spectra, the G band of DH-Zn-ZIF-C shifted to the right-most (~ 1600 cm^{-1}) position, and the G band of ZIF-8-C shifted to the left-most positions (~ 1562 cm^{-1}), which indicated the most n-type doping on nanoporous carbon. In addition, the highest I_D/I_G value of ZIF-8-C also implied the broadened C(002) plane caused by the different bond distances of C-C and C-N, in agreement with the high-resolution TEM, XRD, EDX mapping and XPS results.

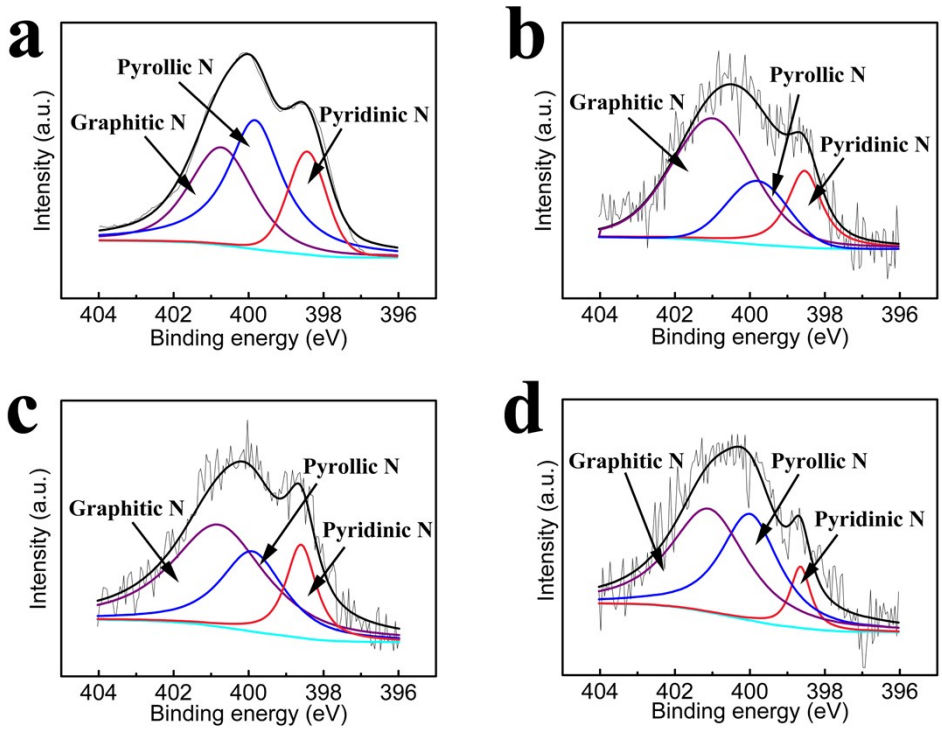

Figure S20 The high-resolution N 1s XPS spectra of ZIF-8-C (a), 3D Ni-MOF-74@ZIF-8-C (b), 2D ZnCo-TCPP@ZIF-8-C (c) and 1D ZnCo-MOF-74@ZIF-8-C (d). Each spectra could be fitted with three peaks at approximately 398.5, 399.8 and 400.8 eV, corresponding to pyridinic N, pyrrolic N and graphitic N, respectively. The N doping of these nanoporous carbon stemmed from carbonization of ZIF liagnds (N-containing imidazole rings), and the incorporation of heteroatom N into carbon lattice could enlarge the interlayer spacing of C(002) and offer more active sites for absorbing K^+ ions, which is beneficial to the excellent K^+ storage performance.

Table S1 The N-doping content of ZIF-8-C, Ni-MOF-74@ZIF-8-C, ZnCo-TCPP@ZIF-8-C and ZnCo-MOF-74@ZIF-8-C detected by XPS analysis; the specific content of pyridinic N, pyrrolic N and graphitic N extracted from Figure S20.

Materials	Overall N	Pyridinic N	Pyrrolic N	Graphitic N
ZIF-8-C	10.42%	2.01%	4.85%	3.56%
Ni-MOF-74@ZIF-8-C	4.31%	0.84%	0.88%	2.59%
ZnCo-TCPP@ZIF-8-C	5.16%	0.84%	1.51%	2.81%
ZnCo-MOF-74@ZIF-8-C	4.61%	0.38%	1.87%	2.36%

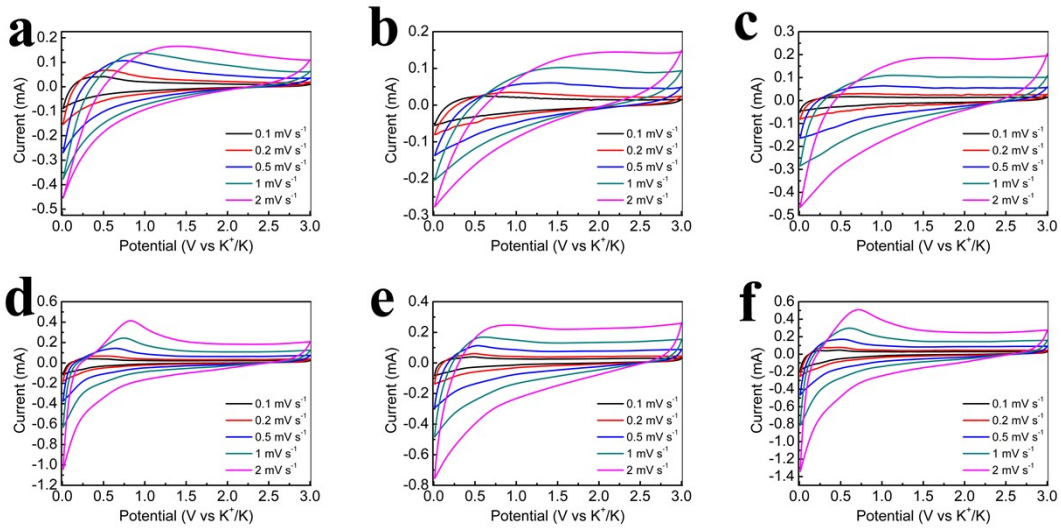

Figure S21 CV plots of ZIF-8-C (a), Ni-MOF-74-C (b), ZnCo-TCPP-C (c), ZnCo-MOF-74-C (d), Ni-MOF-74@ZIF-8-C (e) and ZnCo-TCPP@ZIF-8-C (f) at different scan rates.

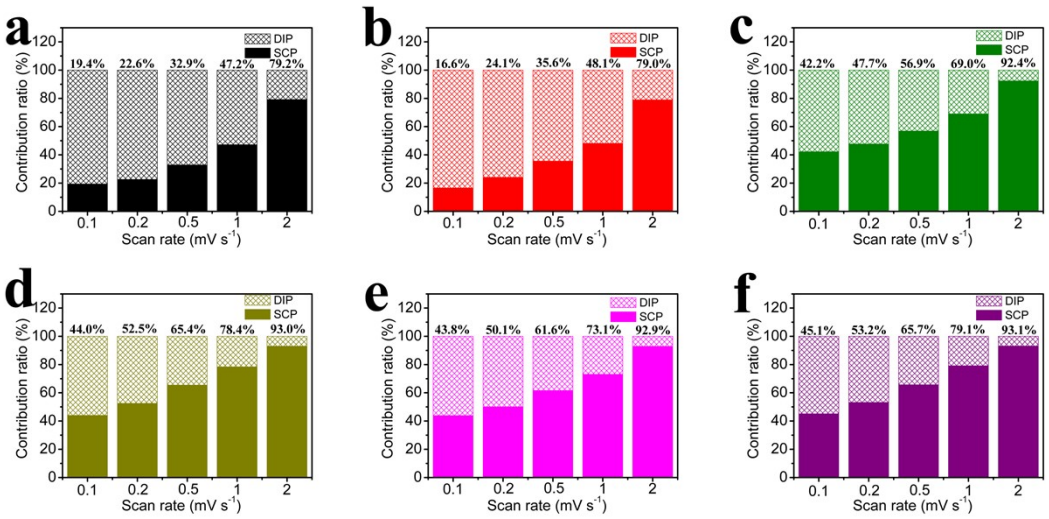

Figure S22 Contribution ratio of DIP and SCP versus scan rate calculated from CV plots of ZIF-8-C (a), Ni-MOF-74-C (b), ZnCo-TCPP-C (c), ZnCo-MOF-74-C (d), Ni-MOF-74@ZIF-8-C (e) and ZnCo-TCPP@ZIF-8-C (f). The specific contribution percentage values of SCP were indicated in each diagram.

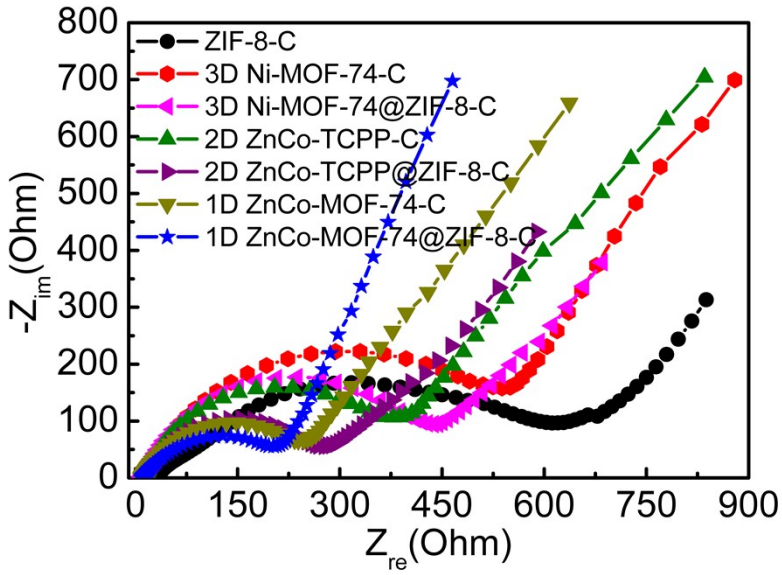

Figure S23 Nyquist plots of ZIF-8-C, 3D Ni-MOF-74-C, 3D Ni-MOF-74@ZIF-8-C, 2D ZnCo-TCPP-C, 2D ZnCo-TCPP@ZIF-8-C, 1D ZnCo-MOF-74-C and 1D ZnCo-MOF-74@ZIF-8-C at a range of 0.1 Hz ~ 100 kHz.

Table S2 K^+ storage properties of MOF-derived carbon materials in recent literature.

Materials	Specific Capacity	Rate Capability	Cycling Stability	References
Cu-MOF-derived N-doped porous carbon nanosheets	276 mAh g^{-1} at 50 mA g^{-1}	184 mAh g^{-1} at 1 A g^{-1} ; 157 mAh g^{-1} at 2 A g^{-1}	94.5% after 6000 cycles at 1 A g^{-1}	*Angew. Chem. Int. Ed.*, **2020**, 59, 19460
Mn-MOF derived porous carbon	266.4 mAh g^{-1} at 50 mA g^{-1}	119.3 mAh g^{-1} at 1 A g^{-1} ; 93 mAh g^{-1} at 2 A g^{-1}	~ 100% after 1000 cycles at 0.2 A g^{-1}	*Adv. Funct. Mater.*, **2020**, 30, 2006561.
MIL-100-derived S/N co-doped thin carbon	320 mAh g^{-1} at 50 mA g^{-1}	123.5 mAh g^{-1} at 1 A g^{-1} ; 91.2 mAh g^{-1} at 2 A g^{-1}	71.3% after 900 cycles at 2 A g^{-1}	*Adv. Mater.*, **2019**, 31, 1805430.
Cu-BTC-derived N/O co-doped carbon	354 mAh g^{-1} at 50 mA g^{-1}	110 mAh g^{-1} at 1 A g^{-1}	90.9% after 1300 cycles at 1 A g^{-1}	*J. Mater. Chem. A*, **2019**, 7, 12317.
MIL-101-derived N/O dual-doped hard carbon	365 mAh g^{-1} at 25 mA g^{-1}	118 mAh g^{-1} at 3 A g^{-1}	69.5% after 1100 cycles at 1.05 A g^{-1}	*Adv. Mater.*, **2018**, 30, 1700104.
ZIF-67-derived N-doped porous carbon	587.6 mAh g^{-1} at 50 mA g^{-1}	207.8 mAh g^{-1} at 1 A g^{-1} ; 186.2 mAh g^{-1} at 2 A g^{-1}	39.4% after 2000 cycles at 0.5 A g^{-1}	*J. Mater. Chem. A*, **2018**, 6, 17959.
Macroporous ZIF-8 single crystal- derived N-doped porous carbon	345 mAh g^{-1} at 100 mA g^{-1}	180 mAh g^{-1} at 1 A g^{-1} ; 94 mAh g^{-1} at 10 A g^{-1}	105.4% after 12000 cycles at 2 A g^{-1}	*Nano Lett.*, **2019**, 19, 4965
Hollow ZIF-8-derived carbon nanobubbles	330 mAh g^{-1} at 50 mA g^{-1}	100 mAh g^{-1} at 100 mA g^{-1}	76.9% after 50 cycles at 1 A g^{-1}	*Chem. Sci.*, **2017**, 8, 3538
Zn-MOF@Co-MOF nanosheet-derived carbon	310 mA h g^{-1} at 100 mA g^{-1}	170 mAh g^{-1} at 2 A g^{-1}; 120 mAh g^{-1} at 5 A g^{-1}	89.3% after 5200 cycles at 1 A g^{-1}	*J. Mater. Chem. A*, **2019**, 7, 19929
Al-MIL-NH_2 nnaorod-derived N-doped carbon	305 mA h g^{-1} at 100 mA g^{-1}	202 mAh g^{-1} at 1 A g^{-1}; 162 mAh g^{-1} at 6 A g^{-1}	~ 100% after 500 cycles at 6 A g^{-1}	*Small*, **2021**, 17, 2100135
MIL-88A-derived S-doped carbon	358.4 mAh g^{-1} at 50 mA g^{-1}	192.6 mAh g^{-1} at 2 A g^{-1}	90.9% after 700 cycles at 1 A g^{-1}	*ACS Appl. Energy Mater.*, **2021**, 4, 2282
ZIF-67-derived N-doped carbon nanotubes	254.7 mAh g^{-1} at 50 mA g^{-1}	180 mAh g^{-1} at 0.5 A g^{-1}; 131 mAh g^{-1} at 2 A g^{-1}	77.86% after 500 cycles at 2 A g^{-1}	*ChemSusChem*, **2018**, 11, 202
1D ZnCo-MOF-74 @ZIF-8-C carbon nanowires	**389.8 mAh g^{-1} at 100 mA g^{-1}**	**196.7 mAh g^{-1} at 1 A g^{-1} ; 163.1 mAh g^{-1} at 2 A g^{-1}; 138.3 mAh g^{-1} at 3 A g^{-1}**	**91.9%, 83.6% and 80.7% after 1000, 1500 and 2000 cycles at 1 A g^{-1}**	**Our work**

Table S3 K^+ storage properties of other carbon materials in recent literature.

Materials	Specific Capacity	Rate Capability	Cycling Stability	References
Ag/PPy-derived porous carbon nanotube aerogels	253.7 mAh g^{-1} at 50 mA g^{-1}	193.3 mAh g^{-1} at 1 A g^{-1}	88.7 % after 1000 cycles at 70 mA g^{-1}	*ACS Appl. Mater. Interfaces*, **2020**, 12, 27045
N/O dual-doped hard carbon	439.1 mAh g^{-1} at 100 mA g^{-1}	254.4 mAh g^{-1} at 1 A g^{-1} ; 223.4 mAh g^{-1} at 2 A g^{-1}	74.5% after 5000 cycles at 1 A g^{-1}	*Adv. Sci.*, **2020**, 7, 1902547.
N/S dual-doped graphitic hollow architectures	≈ 220 mAh g^{-1} at 500 mA g^{-1}	192 mAh g^{-1} at 1 A g^{-1} ; 155 mAh g^{-1} at 2 A g^{-1}	90.2% after 5000 cycles at 5 A g^{-1}	*Adv. Energy Mater.*, **2020**, 10, 2001161.
Polyaniline-*co*-polypyrrole-derived N-doped carbon	423 mAh g^{-1} at 50 mA g^{-1}	195 mAh g^{-1} at 1 A g^{-1} ; 148 mAh g^{-1} at 2 A g^{-1}	93.8% after 660 cycles at 0.2 A g^{-1}	*Angew. Chem. Int. Ed.*, 2020, 59, 4448
Superabsorbent polymers-derived porous carbon	291.9 mAh g^{-1} at 50 mA g^{-1}	151.4 mAh g^{-1} at 1 A g^{-1} ; 136.7 mAh g^{-1} at 2 A g^{-1}	106.8% after 2000 cycles at 1 A g^{-1}	*J. Power Sources*, **2020**, 451, 227727.
Nitrogen-doped turbostratic carbon	518 mAh g^{-1} at 50 mA g^{-1}	212 mAh g^{-1} at 2 A g^{-1} ; 119 mAh g^{-1} at 5 A g^{-1}	93.1% after 500 cycles at 1 A g^{-1}	*Adv. Mater.*, **2020**, 32, 2000732.
Crustacean-derived hard carbon porous nanobelts	468 mAh g^{-1} at 50 mA g^{-1}	235 mAh g^{-1} at 1.6 A g^{-1}	≈ 100% after 1600 cycles at 1 A g^{-1}	*Nano Energy*, **2020**, 77, 105018.
Silicon carbide - derived carbon	289.9 mAh g^{-1} at 100 mA g^{-1}	197.3 mAh g^{-1} at 1 A g^{-1}	89.3% after 1000 cycles at 1 A g^{-1}	*Adv. Funct. Mater.*, **2020**, 30, 2004348.
Acetonitrile-derived porous carbon	271 mAh g^{-1} at 50 mA g^{-1}	135 mAh g^{-1} at 1 A g^{-1} ; 98 mAh g^{-1} at 5 A g^{-1}	82% after 600 cycles at 0.1 A g^{-1}	*J. Power Sources*, **2020**, 466, 228303.
Ni-EDTA compound compound-derived N-doped carbon	369 mAh g^{-1} at 50 mA g^{-1}	152 mAh g^{-1} at 1 A g^{-1} ; 123 mAh g^{-1} at 2 A g^{-1}	82% after 200 cycles at 0.2 A g^{-1}	*Adv. Funct. Mater.*, **2019**, 29, 1903641.
Multiwalled hierarchical carbon nanotube	232 mAh g^{-1} at 0.1 A g^{-1}	162 mAh g^{-1} at 1.6 A g^{-1}	90% after 500 cycles at 0.1 A g^{-1}	*Adv. Mater.*, **2018**, 30, 1802074.
Amorphous ordered mesoporous carbon	286.4 mAh g^{-1} at 50 mA g^{-1}	144.2 mAh g^{-1} at 1 A g^{-1}	101.6% after 1000 cycles at 1 A g^{-1}	*Adv. Energy Mater.*, **2018**, 8, 1701648.

N-doped bamboo-like carbon nanotubes	359 mAh g^{-1} at 100 mA g^{-1}	186 mAh g^{-1} at 1 A g^{-1}	84.6% after 1000 cycles at 0.5 A g^{-1}	J. Mater. Chem. A, 2018, 6, 15162
porous yolk-shell carbon sphere	314 mAh g^{-1} at 50 mA g^{-1}	155 mAh g^{-1} at 1 A g^{-1} ; 134 mAh g^{-1} at 2 A g^{-1}	93.9% after 1200 cycles at 1 A g^{-1}	*J. Mater. Chem. A*, **2018**, 6, 23318
PPy nanofiber - derived N-doped carbon	238 mAh g^{-1} at 100 mA g^{-1}	172 mAh g^{-1} at 1 A g^{-1} ; 153 mAh g^{-1} at 2 A g^{-1}	95.3% after 2000 cycles at 1 A g^{-1}	*Nat. Commun.*, **2018**, 9, 1720.
Hierarchically N-doped porous carbon	381.7 mAh g^{-1} at 0.05 A g^{-1}	185.0 mAh g^{-1} at 10 A g^{-1}	88.3% after 1000 cycles at 1.0 A g^{-1}; 86.0% after 1000 cycles at 2.0 A g^{-1}	*Adv. Energy Mater.*, **2018**, 8, 1802386
1D ZnCo-MOF-74 @ZIF-8-C carbon nanowires	**523.2 mAh g^{-1} at 50 mA g^{-1}; 389.8 mAh g^{-1} at 100 mA g^{-1}**	**196.7 mAh g^{-1} at 1 A g^{-1} ; 163.1 mAh g^{-1} at 2 A g^{-1}; 138.3 mAh g^{-1} at 3 A g^{-1}**	**91.9%, 83.6% and 80.7% after 1000, 1500 and 2000 cycles at 1 A g^{-1}**	**Our work**